EAST EUROPEAN JOURNAL OF PHYSICS. **2.** 373-378 (2026)
DOI:10.26565/2312-4334-2026-2-40 ISSN 2312-4334

FABRICATION AND ELECTRICAL TRANSPORT PROPERTIES OF TRIPLE-BARRIER GaAs-BASED M–p–n–M STRUCTURES

Bahodir M. Abdukahhorov, Oybek A. Abdulkhaev, Damir B. Istamov*, Shukurullo M. Kuliyev, Dilbara M. Yodgorova
Physical-Technical Institute of Uzbekistan Academy of Sciences, Tashkent 100084, Uzbekistan
**Corresponding Author e-mail: istamov@uzsci.net*
Received February 28, 2026; revised March 31, 2026; April 16, 2026

Engineering multi-barrier potential profiles provides an effective approach to controlling charge-carrier transport in semiconductor structures. In this work, three configurations of triple-barrier *GaAs*-based metal–p–n–metal (M–p–n–M) structures were fabricated on semi-insulating *GaAs* substrates using liquid phase epitaxy (LPE). The layer composition and semitransparent metal contacts (*Ag*, *Au*) were deliberately designed to form a coupled system of metal–semiconductor and *p* - *n* junctions. The electrical transport properties were investigated over a wide voltage range, and the current–voltage characteristics were comparatively analyzed. In the low-bias regime, the current follows a power-law dependence $I \sim V^{0.5}$, indicating generation-dominated transport. With increasing bias, a transition to a quasi-ohmic region and subsequent breakdown behavior was observed. In the high-field regime, linear regions in the $ln(I/U^2)$ versus $1/U$ dependence confirm the dominance of field-assisted transport mechanisms within the barrier regions. The results demonstrate that electric-field redistribution and barrier coupling play key roles in governing charge transport in triple-barrier structures, providing a foundation for the further development of advanced semiconductor devices.
Keywords: *Gallium arsenide; Metal–semiconductor junction; p–n junction; Triple-barrier structure; Liquid phase epitaxy; Electrical transport; High-field effects*
PACS: 73.40.Sx, 73.40.-c, 72.20.Ht, 72.20.Jv, 85.60.Gz

1. INTRODUCTION

The rapid development of optical communication and high-speed signal processing systems requires photodetector architectures that combine low dark current, high responsivity, and a wide operational voltage range[1–6]. Gallium arsenide ($GaAs$)-based metal-semiconductor-metal (MSM) photodetectors offer intrinsic advantages such as low capacitance and fast response. However, their performance is often limited by relatively low Schottky barrier heights, which lead to increased dark current levels [7–10]. In addition, the high density of surface states in $GaAs$ can give rise to surface leakage currents, further degrading sensitivity [11–13].

Traditional photoresistors previously employed in optoelectronic circuits have largely been replaced by semiconductor photostructures based on $p-n$ junctions. Avalanche photodiodes, $p-i-n$ photodiodes, and phototransistors with internal gain mechanisms are widely used in high-speed and high-sensitivity applications [14–18]. Such devices can also operate in unconventional biasing modes to enable advanced functional capabilities [19].

For ultraviolet and visible spectral regions ($200 \div 900\ nm$), photodetectors are typically fabricated using compound semiconductors such as GaP, $GaAsP$, and $GaAs$ [20,21]. Various contact metals, including Au [22], Pt [23], Ni [24], Al [25], and Cu [26], are employed to tailor metal-semiconductor interfaces. The introduction of thin interfacial insulating layers has been shown to suppress reverse leakage currents and increase breakdown voltages without significantly compromising photosensitivity.

In recent years, several approaches have been proposed to mitigate dark current and enhance performance, including modified Schottky contacts, nBn architectures, and double-barrier heterostructures [27–29]. In multi-barrier systems, the sequential limitation of current by individual junctions enables improved control over breakdown processes and reduced leakage currents.

High-field carrier transport in barrier structures is commonly described within the Fowler–Nordheim tunneling framework [30], while charge transport across thin potential barriers can be further interpreted using the Simmons model [31].

Owing to its direct bandgap, high electron mobility, and stable metal-semiconductor interface formation, $GaAs$ remains one of the most attractive compound semiconductors for photodetectors and photovoltaic applications [7,32].

Despite these advances, most reported MSM and heterostructure devices rely on nanostructuring, plasmonic enhancement, or complex epitaxial techniques. In contrast, the electrophysical behavior of classical multi-barrier $M-p-n-M$ architectures fabricated by liquid phase epitaxy (LPE) have not been systematically investigated. In particular, the role of controlled $p-$layer thickness in barrier coupling and in the transition between transport regimes under high electric fields has not been experimentally clarified.

In this context, the present study is focused on electrical transport under dark conditions as a fundamental step toward understanding carrier dynamics in multi-barrier semiconductor structures.

Cite as: B.M. Abdukahhorov, O.A. Abdulkhaev, D.B. Istamov, Sh.M. Kuliyev, D.M. Yodgorova, East Eur. J. Phys. 2, 373 (2026), https://doi.org/10.26565/2312-4334-2026-2-40

The objective of this work is to develop baseline structural designs and fabrication technologies for semiconductor structures, to fabricate experimental samples, and to elucidate the mechanisms governing their electrical transport properties.

In this study, triple-barrier $GaAs$-based $M-p-n-M$ structures were fabricated by liquid phase epitaxy, and their carrier transport mechanisms in the high-field regime were comparatively analyzed based on current–voltage characteristics.

2. STRUCTURE AND FABRICATION

2.1 Structural Design of Triple-Barrier $m-p-n-m$ structures

The investigated structures were designed as triple-barrier $metal-p-n-metal$ ($M-p-n-M$) architectures fabricated on semi-insulating (SI) $GaAs$ substrates (Fig. 1). The structure consists of a top metal-semiconductor ($M-S$) junction, a central $p-n$ junction, and a bottom metal–semiconductor junction, thereby forming three sequentially coupled potential barriers. Such a configuration enables electric field redistribution across the layers under applied bias and promotes inter-barrier coupling effects.

Figure 1. Structural concept and electrical measurement configuration of the fabricated triple-barrier $m-p-n-m$ $GaAs$-based structures: (a) layered schematic representation of the vertical architecture, and (b) planar cross-sectional view illustrating the coupled metal-semiconductor and p-n junctions.

(100)-oriented $SI\ GaAs$ single-crystal substrates were employed, with a carrier concentration of approximately $2.0\times10^{8}\ cm^{-3}$ and a thickness of 350 µm. Three sample types (Sample-01, Sample-02, and Sample-03) were fabricated, differing in layer sequence, conductivity type, and homo-/heterojunction configuration (Table 1). The epitaxial layer thickness ranged from 1.2 to 2 µm, with the p-layer intentionally designed to be significantly thinner than the n-type base region.

2.2 Liquid Phase Epitaxy Growth Parameters

The epitaxial layers were grown by liquid phase epitaxy (LPE) using a graphite boat system with a sliding (shift) mechanism (Fig. 2). Growth was carried out in a purified hydrogen (H_2) ambient. Crystallization was initiated at approximately 860 °C, and the cooling rate was carefully controlled within the range of $0.33-0.4$ °C/min. This slow cooling regime ensured a stable supersaturation level in the melt and promoted uniform layer formation.

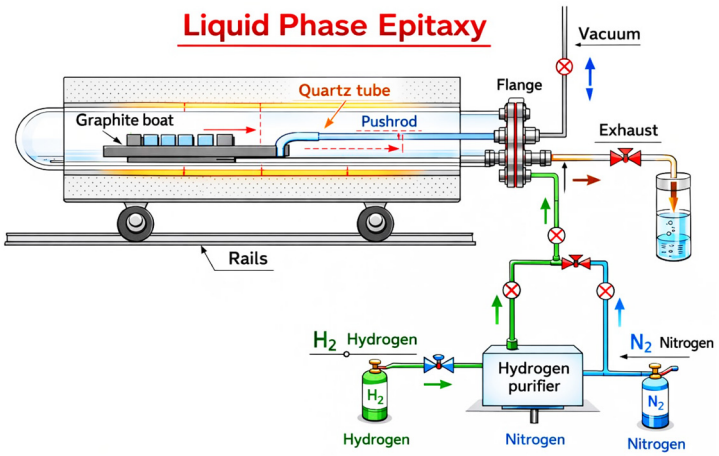

Figure 2. Schematic diagram of the liquid phase epitaxy (LPE) system used for the growth of triple-barrier GaAs-based m-p-n-m structures, showing the graphite boat assembly, quartz tube reactor, gas flow control (H_2/N_2), and sliding mechanism for controlled melt-substrate interaction.

Table 1. Structural parameters of fabricated triple-barrier $m-p-n-m$ $GaAs$-based structures

No.	Sample ID	Layer Sequence	Conductivity Type	Contact Metals	Barrier Configuration
1	Sample -01	$Ag-nGaAs-\pi GaAs-Ag$	$n\ /\ p^{-}$	$Ag\ /\ Ag$	$M-S\ /\ n-p\ /\ S-M$
2	Sample-02	$Ag-nAlxGa_{1-x}-As-\pi GaAs-Ag$	$n\ /\ p$	$Ag\ /\ Ag$	$M-S\ /\ n-p\ /\ S-M$
3	Sample -03	$Au-pAlInGaAs-\nu GaAs-Au$	$p\ /\ n^{-}$	$Au\ /\ Au$	$M-S\ /\ p-n\ /\ S-M$

For n −type layers, the melt composition consisted of $Ga + nGaAs{:}\,Sn + Al$, whereas p −type layers were formed from $Ga +\ pGaAs{:}\,Zn + Al$ solutions. The growth duration followed the relation $\Delta t_n = 1.7 \times 2^n$ $(n = 1 \div 4)$.

The dopant concentration in the epitaxial layers was at least $2 \times 10^{15}\mathrm{cm}^{-3}$; Sn-doped sources exhibited concentrations $\leq 2 \times 10^{15}\mathrm{cm}^{-3}$, while Zn-doped sources reached approximately $5 \times 10^{17}\mathrm{cm}^{-3}$.

The intentionally reduced p −layer thickness facilitates the coupling of adjacent space-charge regions under high electric fields, which subsequently influences the transition of the dominant transport mechanism.

2.3 Contact Formation and Device Geometry

Metal contacts were deposited onto the epitaxial surface by vacuum evaporation. A semitransparent rectifying contact (Ag or Au) with a thickness of approximately 70 Å was formed on the top epitaxial layer. An identical semitransparent (~70 Å) rectifying metal layer was deposited on the backside of the substrate.

These symmetric metal–semiconductor interfaces establish two Schottky-type barriers that, together with the central $p - n$ junction, complete the triple-barrier $M - p - n - M$ configuration. The ultrathin semitransparent contacts preserve carrier injection characteristics while enabling efficient electric field redistribution within the structure.

The active device area ranged from 2 to 25 mm^2, with some samples fabricated up to 1×1 cm^2. The n-type base thickness was 350 μm, whereas the epitaxial layer thickness was $1.2 - 2$ μm.

3. Electrical Measurement Method

The current-voltage (I-V) characteristics were measured under dark and illumination conditions using a standard two-probe configuration. The bias voltage was applied and controlled by a Keithley 2460 SourceMeter with a step increment of 0.05 V. Current and voltage values were recorded using the instrument's high-precision internal measurement modules.

The minimum detectable current was 0.1 nA. The relative measurement uncertainty ranged between 0.2-0.4%, determined by the metrological specifications of the Keithley 2460 system.

Measurements in the breakdown region were performed in current-stabilization mode using the built-in current source and protection functions of the instrument to ensure device safety and data reliability.

4. RESULTS

4.1 Current–Voltage Characteristics

The current-voltage $(I - V)$ characteristics of the fabricated triple-barrier $M - p - n - M$ structures are presented in Fig. 6. All samples (Sample-01, Sample-02, and Sample-03) exhibit pronounced nonlinear current-voltage behavior, which originates from the sequential arrangement of two metal–semiconductor $(M - S)$ junctions and one central $p - n$ junction.

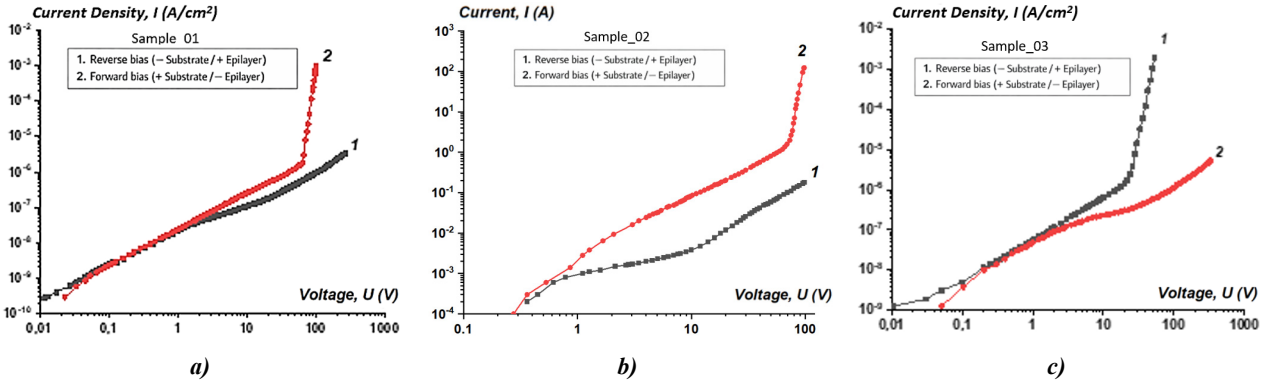

Figure 3. Dark current-voltage $(I - V)$ characteristics of the fabricated triple-barrier $m - p - n - m$ GaAs-based photostructures: (a) Sample-01 (homojunction, p-type substrate), (b) Sample-02 (heterojunction, p-type substrate), and (c) Sample-03 (homojunction, n-type substrate).

Under dark conditions, the $I - V$ characteristics reflect the collective response of the three coupled barriers. In the low-bias region, the current follows a power-law dependence $I{\sim}V^{0.5}$, indicating the dominance of generation processes in the reverse-biased junction. As the applied voltage increases, a broad ohmic region emerges. Beyond a characteristic voltage U_0, a sharp current rise (breakdown region) appears in only one bias polarity.

A notable feature common to all structures is that breakdown consistently initiates when the current density reaches approximately $J \approx 1$ $\mu\mathrm{A/cm}^2$.

The breakdown voltage U_{br} depends on the thickness of the base region, with thinner bases leading to lower breakdown voltages. Furthermore, the polarity at which breakdown occurs is governed by the conductivity type of the substrate.

4.2 High-Field Transport Analysis

In the breakdown region, the dependence $ln(I/U^2) \sim 1/U$ exhibits clear linear behavior for all samples (Fig. 7), supporting the hypothesis of a tunneling-dominated breakdown mechanism. Although slope values were not explicitly extracted, the observed linearity indicates that field-assisted carrier transport across the barrier becomes dominant at high electric fields.

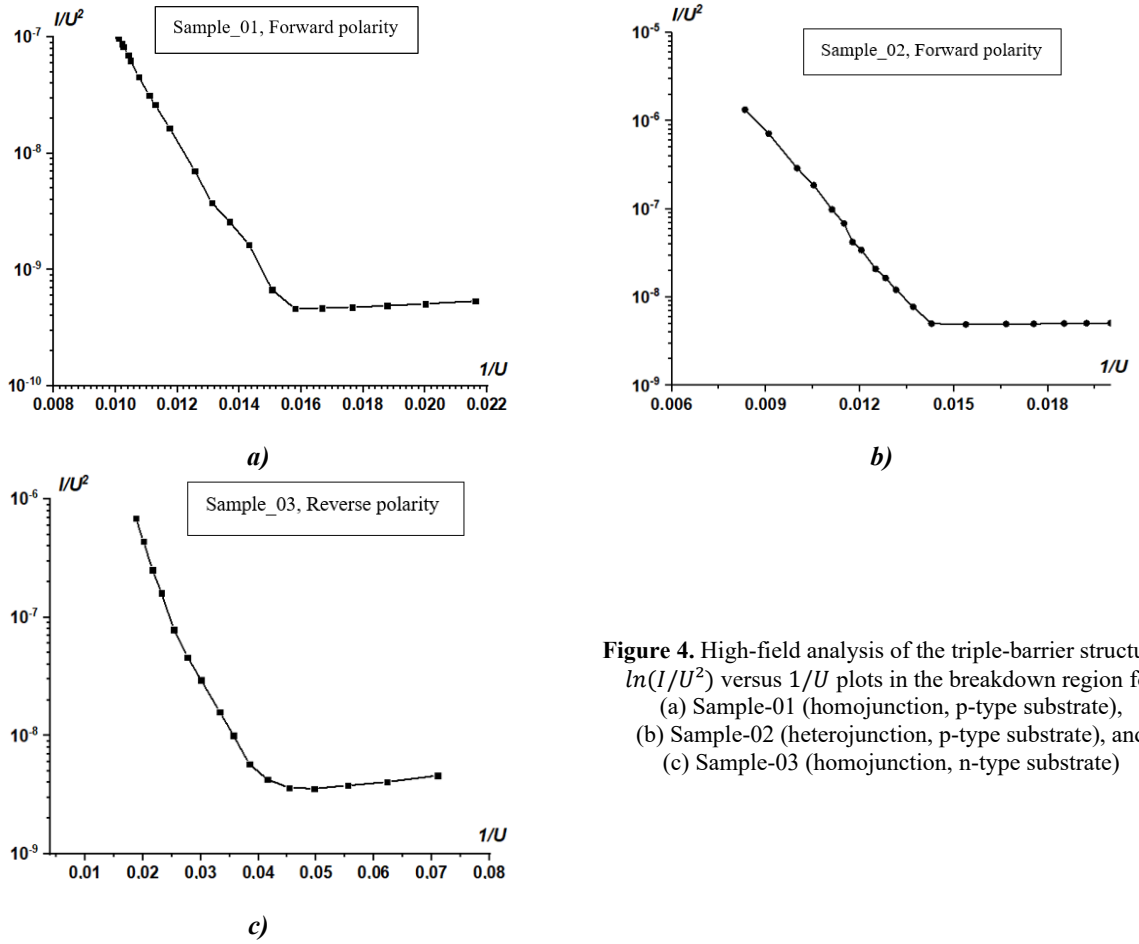

Figure 4. High-field analysis of the triple-barrier structures: $ln(I/U^2)$ versus $1/U$ plots in the breakdown region for (a) Sample-01 (homojunction, p-type substrate), (b) Sample-02 (heterojunction, p-type substrate), and (c) Sample-03 (homojunction, n-type substrate)

The triple-barrier structure is model-wise analogous to a thyristor; however, it differs due to the presence of a thick n −type base (≈ 350 μm) and a comparatively thinner secondary region. This configuration promotes the coupling (merging) of adjacent space-charge regions prior to the onset of avalanche multiplication. As a result, the wide ohmic region and the occurrence of breakdown in only one bias regime represent characteristic features of the multi-barrier architecture.

5. SHORT DISCUSSION

The obtained results reveal that increasing bias voltage in the triple-barrier $M - p - n - M$ architecture leads to a pronounced redistribution of the electric field across the layered structure. In the low-voltage regime, the current follows a $I \sim V^{0.5}$ dependence, indicating the predominance of generation–recombination processes in the reverse-biased junction. With further increases in voltage, the influence of the blocking junction becomes dominant, and the structure transitions into an extended ohmic region.

The combination of a thin p −layer and a relatively thick n −type base facilitates the convergence of adjacent space-charge regions. At a critical bias, these regions couple (barrier coupling), resulting in a sharp increase in current. This behavior precedes classical avalanche multiplication and reflects the intrinsic interaction between sequentially connected barriers.

In the breakdown regime, the linear dependence of $ln(I/U^2)$ on $1/U$ indicates the dominance of a tunneling-assisted transport mechanism under high electric fields. Thus, breakdown in the multi-barrier architecture is governed by field-controlled carrier transport, with its characteristics tunable through structural parameters. These features may be of interest for further studies aimed at evaluating the dynamic properties of such structures.

6. CONCLUSIONS

Triple-barrier $GaAs$-based $M - p - n - M$ structures were successfully fabricated using liquid phase epitaxy (LPE). The deliberate selection of structural and technological parameters enabled the formation of a coupled barrier system composed of two metal–semiconductor junctions and a central $p - n$ junction.

The current–voltage characteristics demonstrate generation-dominated transport ($I \sim V^{0.5}$) at low bias and the emergence of a breakdown region under high electric fields. Breakdown consistently occurs when the current density approaches approximately 1 $\mu A/cm^2$, while the breakdown voltage is strongly dependent on the base-region thickness. The observed linearity in the $ln(I/U^2) \sim 1/U$ relation confirms the predominance of tunneling-assisted transport in the high-field regime.

These findings demonstrate that electric field redistribution and barrier coupling are the key mechanisms governing carrier transport in triple-barrier architectures. The proposed structural approach provides a promising platform for advanced semiconductor devices operating under high-field conditions.

ORCID

Oybek A. Abdulkhaev, https://orcid.org/0000-0002-8822-1187; **Damir B. Istamov,** https://orcid.org/0009-0007-4654-1880;
Bahodir M. Abdukahhorov, https://orcid.org/0009-0002-0932-0281

REFERENCES

[1] B. Fang, Y. Tian, and Z. Ma, "High carrier collection efficiency in graphene/GaAs heterojunction photodetectors," J. Semicond. **46**, (2025). https://doi.org/10.1088/1674-4926/24110002
[2] Y. Tian, H. Liu, J. Li, B. Liu, and F. Liu, "Recent Developments of Advanced Broadband Photodetectors Based on 2D Materials," Nanomaterials, **15**, (2025). https://doi.org/10.3390/nano15060431
[3] R.R. Kabulov, L.O. Shuhratova, K.T. Suyarov, F.A. Akbarov, D.B. Istamov, Structural, Compositional, and Photoluminescence Properties of $CsPbBr_3$ Thin Films Grown by Single-source Thermal Vacuum Chemical Vapor Deposition, E-Journal Surf. Sci. Nanotechnol. **367**, 364–367 (2025). https://doi.org/10.1380/ejssnt.2025-051
[4] F. Li, J. Zeng, Y. Zhao, L. Zhu, Y. Zhou, Z. Wang, Z. Wang, *et al*., "High Hole Mobility van der Waals Junction Field-Effect Transistors Based on Te/GaAs for Multimode Photodetection and Logic Applications," ACS Appl. Mater. Interfaces, **17**, 18655-18665 (2025). https://doi.org/10.1021/acsami.5c00891
[5] I.I. Maripov, S.A. Radzhapov, S.F. Xasanov, D.B. Istamov, Y.T. Yuldashev, D. Axnazarova, and S.A. Ashirov, "Electrophysical Characterization of Photodetectors Based on Semiconductor Structures Si (Li) And Si(Au)," East Eur. J. Phys. (4), 435–441 (2025). https://doi.org/10.26565/2312-4334-2025-4-43
[6] E. Balcı, H. Durmuş, Ç. Bilkan, and Ş. Altındal, "On the electrical parameters, conduction mechanisms depend on temperature and voltage, and thermal sensor applications in the Re/n-GaAs/Au Schottky diodes," J. Mater. Sci. Mater. Electron. **37**, (2026). https://doi.org/10.1007/s10854-025-16561-6
[7] F. Lin, J. Cui, Z. Zhang, Z. Wei, X. Hou, B. Meng, Y. Liu, *et al*., "GaAs Nanowire Photodetectors Based on Au Nanoparticles Modification," Materials (Basel). **16**, 1–11 (2023). https://doi.org/10.3390/ma16041735
[8] F. Capasso, "Band-Gap Engineering: From Physics and Materials To New Semiconductor Devices," Science, **235**, 172-176 (1987). https://doi.org/10.1126/science.235.4785.172
[9] A. Rogalski, "Infrared detectors: Status and trends," Prog. Quantum Electron. **27**, 59–210 (2003). https://doi.org/10.1016/S0079-6727(02)00024-1
[10] B.F. Levine, "Quantum-well infrared photodetectors," J. Appl. Phys. **74**, (1993). https://doi.org/10.1063/1.354252
[11] S. Mohammadnejad, and M. Aasi, "Analysis of structures and technologies of various types of photodetectors used in laser warning systems: a review," Opt. Eng. **62**, (2023). https://doi.org/10.1117/1.oe.62.9.090901
[12] H.J. Lee, M.M.A. Gamel, P.J. Ker, M.Z. Jamaludin, Y.H. Wong, and J.P.R. David, "Absorption Coefficient of Bulk III-V Semiconductor Materials: A Review on Methods, Properties and Future Prospects," J. Electron. Mater. **51**, 6082–6107 (2022). https://doi.org/10.1007/s11664-022-09846-7
[13] Z. Sun, "Electron Transport in High Aspect Ratio Semiconductor Nanowires and Metal-Semiconductor Interfaces," 2016. http://rave.ohiolink.edu/etdc/view?acc_num=ucin1479821421998919
[14] D.B. Istamov, O.A. Abdulkhayev, and S.M. Kuliyev, "Limiting characteristics of silicon diode temperature sensors for determining the maximum temperature with specified measurement accuracy," UNEC J. Eng. Appl. Sci. **5**, 63–69 (2025). https://doi.org/10.61640/ujeas.2025.0507
[15] R. Bebitov, O. Abdulkhaev, D. Yodgorova, D. Istamov, G. Khamdamov, S. Kuliyev, J.S. Abdullaev, *et al*., "Potential distribution over temperature sensors of p-n junction diodes with arbitrary doping of the base region," E3S Web Conf. **401**, (2023). https://doi.org/10.1051/e3sconf/202340103062
[16] R.R. Bebitov, O.A. Abdulkhaev, D.M. Yodgorova, D.B. Istamov, G.M. Khamdamov, S.M. Kuliyev, A.A. Khakimov, and A.Z. Rakhmatov, "Dependence of the accuracy of the silicon diode temperature sensors for cryogenic thermometry on the spread of their parameters," Low Temp. Phys. **49**, 256–260 (2023). https://doi.org/10.1063/10.0016843
[17] R.R. Bebitov, O.A. Abdulkhaev, D.M. Yodgorova, D.B. Istamov, S.M. Kuliyev, A.A. Khakimov, A.B. Bobonazarov, and A.Z. Rakhmatov, "Distribution of impurities in base-depleted region of diode temperature sensor," Low Temp. Phys. **50**, 418-424 (2024). https://doi.org/10.1063/10.0025635
[18] D.B. Istamov, O.A. Abdulkhayev, S.M. Kuliyev, N. Abdullayev, S.A. Ashirov, and D.M. Yodgorova, "Temperature Response Curve of Silicon Diode Temperature Sensors," East Eur. J. Phys. (2), 287–291 (2025). https://doi.org/10.26565/2312-4334-2025-2-35
[19] Z. Ma, P. Tang, J. Xue, and J. Zhou, "Enhancing Photoresponse of GaAs-Based Photodetector by Plasmon Grating Structures," Plasmonics, **18**, 1571–1579 (2023). https://doi.org/10.1007/s11468-023-01849-2
[20] A. Komilov, O. Abdulkhaev, Y. Nasrullayev, B. Abdurasulov, and B. Abdukahhorov, "Error Minimization in PV Characterization When Using Unfiltered Light Sources," Appl. Sol. Energy (English Transl. Geliotekhnika), **60**, 179–188 (2024). https://doi.org/10.3103/S0003701X24602059
[21] S.D. Lin, and C.P. Lee, "GaAs metal-semiconductor-metal photodetectors with low dark current and high responsivity at 850 nm," Semicond. Sci. Technol. **17**, 1261–1266 (2002). https://doi.org/10.1088/0268-1242/17/12/309

[22] L. Boudjemila, *et al*., "Study Of Polarization Photosensitiveness of Nanostructured Au-Palladium-N-Gap Schottky Barriers," in: *Handb. XXII Int. Sci. Conf. "Ecology. Human. Soc*." 99–102 (2021). https://doi.org/https://doi.org/10.20535/EHS.2021.233065
[23] S.M. Sze, D.J. Coleman, and A. Loya, "Current transport in metal-semiconductor-metal (MSM) structures," Solid State Electron. **14**, 1209–1218 (1971). https://doi.org/10.1016/0038-1101(71)90109-2
[24] V.P. Maxniy, "UV photodetectors with a Schottky barrier based on Zinc Selenide," Tech. Phys. J. **68**, 123–125 (1998).
[25] H.H. Gullu, D.E. Yıldız, M. Yıldırım, I. Demir, and I. Altuntas, "Electrical characteristics of Al/AlGaAs/GaAs diode with high-Al concentration at the interface," J. Mater. Sci. Mater. Electron. **35**, (2024). https://doi.org/10.1007/s10854-023-11907-4
[26] E.H. Rhoderick, "Metal-Semiconductor Contacts," IEEE Proc. I Solid State Electron Devices, **129**, 1–14 (1982). https://doi.org/10.1049/ip-i-1.1982.0001
[27] A. Rogalski, P. Martyniuk, M. Kopytko, P. Madejczyk, and S. Krishna, "InAsSb-based infrared photodetectors: Thirty years later on," Sensors (Switzerland), **20**, 1–74 (2020). https://doi.org/10.3390/s20247047
[28] V. Gúriaux, A. Nedelcu, and P. Bois, "Double barrier strained quantum well infrared photodetectors for the 3-5 μm atmospheric window," J. Appl. Phys. **105**, 1–9 (2009). https://doi.org/10.1063/1.3143102
[29] B.S. Ma, W.J. Fan, Y.X. Dang, W.K. Cheah, W.K. Loke, W. Liu, D.S. Li, *et al*., "GaInNAs double-barrier quantum well infrared photodetector with the photodetection at 1.24 μm," Appl. Phys. Lett. **91**, 3–5 (2007). https://doi.org/10.1063/1.2767185
[30] R.H. Fowler, and L. Nordheim, "Electron emission in intense electric fields," Proc. R. Soc. London. Ser. A, Contain. Pap. a Math. Phys. Character, **119**, 173–181 (1928). https://doi.org/10.1098/rspa.1928.0091
[31] J.G. Simmons, "Generalized Formula for the Electric Tunnel Effect between Similar Electrodes Separated by a Thin Insulating Film," J. Appl. Phys. **34**, 1793–1803 (1963). https://doi.org/10.1063/1.1702682
[32] F.X. Liang, J.Z. Wang, Z.P. Li, and L.B. Luo, "Near-Infrared-Light Photodetectors Based on One-Dimensional Inorganic Semiconductor Nanostructures," Adv. Opt. Mater. **5**, 1–14 (2017). https://doi.org/10.1002/adom.201700081

ВИГОТОВЛЕННЯ ТА ЕЛЕКТРИЧНІ ТРАНСПОРТНІ ВЛАСТИВОСТІ ТРЬОХБАР'ЄРНИХ СТРУКТУР GaAs ТИПУ M–p–n–M

Баходір М. Абдукахоров, Ойбек А. Абдулхаєв, Дамір Б. Істамов, Шукурулло М. Кулієв, Ділбара М. Йодгорова
Фізико-технічний інститут Академії наук Узбекистану, Ташкент 100084, Узбекистан

Інженерне формування багатобар'єрних потенціальних профілів є ефективним підходом до керування транспортом носіїв заряду в напівпровідникових структурах. У цій роботі виготовлено три конфігурації трьохбар'єрних структур $GaAs$ типу метал–p–n–метал ($M-p-n-M$) на напівізоляційних підкладках $GaAs$ із використанням методу рідкофазної епітаксії (LPE). Склад шарів і напівпрозорі металеві контакти (Ag, Au) були цілеспрямовано підібрані для формування зв'язаної системи переходів метал–напівпровідник і $p-n$. Електричні транспортні властивості досліджувалися в широкому діапазоні напруг, а вольт-амперні характеристики були піддані порівняльному аналізу. У режимі малих напруг струм підкоряється степеневій залежності $I \sim V^{0,5}$, що свідчить про домінування генераційних процесів. Із зростанням напруги спостерігається перехід до квазіомічної області та подальше формування пробою. У режимі високих електричних полів лінійні ділянки залежності $ln(I/U^2)$ від $1/U$ підтверджують домінування польово-асистованих механізмів транспорту в бар'єрних областях. Отримані результати демонструють, що перерозподіл електричного поля та взаємодія бар'єрів відіграють ключову роль у визначенні транспорту носіїв заряду в трьохбар'єрних структурах, забезпечуючи основу для подальшого розвитку перспективних напівпровідникових приладів.

Ключові слова: *арсенід галію; перехід метал–напівпровідник; p–n перехід; трьохбар'єрна структура; рідкофазна епітаксія; електричний транспорт; ефекти високих електричних полів*